Desalination and Water Treatment
www.deswater.com

doi: 10.1080/19443994.2016.1175971

57 (2016) 26461–26471
November

Taylor & Francis
Taylor & Francis Group

Preparation of iron-copper binary oxide and its effective removal on antimony(V) from water

Yongchao Li[a,*], Xiaoxian Hu[a], Bozhi Ren[a], Jian Yue[a], Weichun Yang[b]

[a]*School of Civil Engineering, Hunan University of Science and Technology, Xiangtan 411201, P.R. China, Tel. +86 731 58290052; Fax: +86 731 58290218; emails: nkliyongchao@163.com (Y. Li), 850050828@qq.com (X. Hu), 564975554@qq.com (B. Ren), changshalaosan@163.com (J. Yue)*

[b]*Department of Environmental Engineering, School of Metallurgy and Environment, Central South University, Changsha 410017, P.R. China, Tel. +86 731 88830875; Fax: +86 731 88710171; email: yang220@csu.edu.cn*

Received 25 November 2015; Accepted 25 March 2016

ABSTRACT

Fe-Cu binary oxides with different Fe/Cu molar ratio were synthesized via a facile co-precipitation process and their performance on Sb(V) removal was systematically evaluated. It demonstrated that as-prepared binary oxides possessed better Sb(V) adsorption capacity than both iron oxide and copper oxide. Moreover, the optimum Fe/Cu molar ratio for binary oxides was about 3/1. Sb(V) adsorption on the Fe-Cu binary oxide did follow a pseudo-second-order kinetic model, indicating that chemical sorption played a major role. The adsorption isotherm data gave better fit to the Freundlich model. Furthermore, the Fe-Cu binary oxide showed an adsorption capacity of 191.9 mg g^{-1} at pH 6.0, which was higher than that of many other adsorbents. Coexisting anion SO_4^{2-} and PO_4^{3-} obviously inhibited the Sb(V) removal. In addition, Sb(V) adsorption on the Fe-Cu binary oxide was favorable under acidic condition. Little of Fe and Cu ions were released to water in pH range of 6.0–9.0. After reaction, the morphology of Fe-Cu binary oxide did change significantly and the surface complex was produced.

Keywords: Fe-Cu binary oxide; Preparation; Sb(V) removal; Antimony residue leach liquor

1. Introduction

Antimony (Sb) is metalloid, and belongs to group VA of the periodic table. It is extensively used in alloys, batteries, flame retardants, and power transmission equipment [1]. Antimony and its compounds are considered to be hazardous to human health or even carcinogenic. Thus, they are considered pollutant of priority interest by the USEPA [2]. Recently, as a result of mining processes, industrial accidents, and shooting activities, large quantities of antimony have been released in waters [3,4]. For example, the concentration of dissolved Sb in surface water around the mining areas of China ranged from 4.58 to 29.4 mg L^{-1} [5]. The concentration of Sb in domestic wells in the Dúbrava abandoned mine site reached 126 μg L^{-1} [6], which was far exceeds the drinking water limit (5 μg L^{-1}).

Trivalent and pentavalent inorganic forms of antimony are the most common species in water solution. According to thermodynamic predictions, Sb(V) presents in aerobic condition and Sb(III) persists in anoxic

*Corresponding author.

media regularly. The Sb(V) species exists dominantly as $Sb(OH)_6^-$ when the pH is higher than 3.0. While the Sb(III) mainly exists as $Sb(OH)_3$ in pH range of 2.0–10.0 [1]. Moreover, Sb(III) species are known to be 10 times more toxic than Sb(V) species [7]. However, the solubility of $Sb(OH)_3$ is low and it can bind more strongly than the $Sb(OH)_6^-$ to hydroxides of Fe, Mn, and humic acids in soils and sediment [8–10]. So, Sb (V) has a greater effect on human than Sb(III), and it was chosen as the target contaminant in this study.

Precipitation [11], coagulation/flocculation [12], electrochemical [13], and adsorption [14] methods have been used for the removal of antimony from aqueous solution. Among these methods, adsorption method is one of the most effective choices because of its low cost, simplicity, rapidness, and high efficiency [15]. Significant research has been conducted on antimony adsorption by different kinds of materials. However, the removal ability of antimony using bentonite [16], carbon nanotubes [17], activated carbon [18], and nanoscale zero-valent iron [19] was not good, and the modification of these materials was generally needed. Most recently, iron based oxide was successfully developed as a novel adsorbent with the significance removal of Sb(III) and Sb(V). For example, akaganeite was synthesized by slow hydrolysis of a $FeCl_3$ solution and used to remove antimonate from water [20]. The removal capacity of Sb(V) by Fe-Mn binary oxide was higher than both ferric hydroxide and manganese dioxide [21]. Moreover, the systematical study of Sb(V) adsorption capability exerted by Fe-Zr [22] and Fe-Zn [23] bimetal composites was also conducted.

As a cheap metal oxide, copper oxide provided wide prospects in gas sensors, solar cells, and catalyst [24,25]. Recently, it was reported that cupric oxide was an effective sorbent for both As(V) and As(III) removal over a wide pH range [26]. Also, Fe-Cu binary oxides were synthesized and tested for arsenic [27] and phosphate [28] removal. Although antimony has chemical similarities to arsenic, copper oxide has seldom been studied for antimony removal from water. It was expected that incorporation of copper into iron oxides would benefit from both the iron oxides and copper oxides.

In this study, a facile co-precipitation method was established to prepare an innovative Fe-Cu binary oxide. The main objectives of this research were to (i) characterize the prepared Fe-Cu binary oxide with a variety of techniques, (ii) optimize the Fe/Cu molar ratio of binary oxides for the Sb(V) adsorption, (iii) investigate Sb(V) removal performance as well as the effect of solution pH and coexisting anions, and (iv) evaluate the potential use of the Fe-Cu binary oxide to treat antimony residue leach liquor.

2. Experimental section

2.1. Chemicals

Iron chloride hexahydrate was purchased from Xilong Chemical Co., Ltd, Guangzhou, China. Cupric sulfate and sodium hydroxide were purchased from Tianjin Yongda Chemical Reagent Co., Ltd, China. Potassium pyroantimonate ($KSb(OH)_6$) was from Aladdin Industrial Corporation, Shanghai, China. Sodium carbonate anhydrous was from Tianjin Chemical Reagent Research Institute Co., Ltd, China. Sodium sulfate anhydrous was purchased from Tianjin Kemiou Chemical Reagent Co., Ltd, China. Sodium phosphate tribasic was from Tianjin Fengchuan Chemical Reagent Science And Technology Co., Ltd, China. All the chemicals and reagents used were analytical grade. Deionized (DI) water was used to prepare stock solutions and synthetic water. Prior to use, all polyethylene bottles, glassware, and sample vessels were immersed in 15% HNO_3 solution, and rinsed with DI water three times.

2.2. Preparation of Fe-Cu binary oxide

Preparation steps of the Fe-Cu binary oxide with a Fe/Cu molar ratio of 2/1 was as follows. First, 12.5 mL of 0.617 mol L^{-1} $FeCl_3$ and 7.5 mL of 0.5 mol L^{-1} $CuSO_4$ solutions were mixed. Then, 1.25 mol L^{-1} NaOH was slowly added into the mixed solution with continuously magnetic stirring. And the solution pH was kept in the range of 9.0–9.5. After addition, the formed suspension was continuously stirred for 2 h, then the suspension was centrifuged at 7,000 r min^{-1} for 10 min, and the deposit was washed with DI water. Fe-Cu binary oxides with a Fe/Cu molar ratio of 1/2, 1/1, and 3/1 were also prepared by altering quantity of $FeCl_3$ and $CuSO_4$. Copper oxide and iron oxide were synthesized using similar methods without adding $FeCl_3$ or $CuSO_4$. The final product was dried at 80°C for 24 h, and ground for 0.5 h with a mortar and pestle. The final dry materials appeared in the form of fine powder and was used for material characterization and Sb(V) removal.

2.3. Characterization of Fe-Cu binary oxide

Particle size and morphology were characterized using scanning electron microscopy (SEM, JSM-6380LV, JEOL, Japan). Chemical composition and

crystal structure were examined by energy-dispersive X-ray spectroscopy (EDX, JSM-6490, JEOL, Japan) and X-ray diffraction (XRD, D8 Advance, Bruker, Germany). Specific surface area was measured by the Brunauer–Emmett–Teller (BET) isotherm using a NOVA2200e surface area and pore size analyzer (Quantachrome Instruments, USA) after degassing the samples at 150°C for 12 h. Functional groups on the surface of prepared sample was measured by Fourier transform infrared (FTIR, Nicolet 6700, USA) spectra with the standard KBr disk method. Zeta potential of sample at different pH was determined using a JS94H micro-electrophoresis apparatus, which was manufactured by the digital technology equipment of Zhongchen Co., Ltd, Shanghai, China.

2.4. Batch adsorption experiment

A Sb(V)-stock solution with an antimony concentration of 100 mg L^{-1} was prepared by dissolving $KSb(OH)_6$ into 2 mol L^{-1} HCl solution. Experimental solutions of Sb(V) were obtained by dilution from the stock solution into DI water. Batch experiments were carried out in 125-mL polypropylene bottles at room temperature (23 ± 1°C). To find out the optimum Fe/Cu molar ratio for binary oxide, 0.03 g of binary oxide with different Fe/Cu molar ratio, pure iron oxide, and copper oxide was added to 100 mL of 20 mg L^{-1} Sb(V) solution with initial pH of 6.0 and then placed on a rotary shaker at 100 r min^{-1}, respectively. At timed intervals, 3 mL aliquots were taken from the suspension, then filtered through 0.45-μm membrane filters and analyzed for total antimony remaining in the aqueous phase. Removal percentage was calculated from Eq. (1):

$$\text{Removal percentage} = \frac{c_0 - c_t}{c_0} \times 100\% \quad (1)$$

where c_0 and c_t are the initial and residual Sb concentrations in the solution (mg L^{-1}).

For kinetics studies, experiments were carried out to view the influence of reaction time on the Sb(V) removal. The Fe-Cu binary oxide (0.01–0.04 g) was added to 100 mL of 40 mg L^{-1} Sb(V) solution at the pH of 6.0. Samples were taken at the following intervals: 0.5, 1, 2, 4, 6, 10, 12, and 24 h of the reaction, and then filtered to determine the residual Sb concentrations in water.

For isothermal adsorption experiments, 0.03 g of Fe-Cu binary oxides was added to 100 mL of solution with initial Sb(V) concentration ranged from 10 to 90 mg L^{-1}. After 48 h of reaction, the residual Sb concentration in solution was determined as mentioned above.

To test the effect of solution pH on Sb(V) adsorption and chemical stability of Fe-Cu binary oxide, the initial pH of Sb(V) solution was pre-adjusted to a desired level from 4.0 to 10.0 with 1.0 mol L^{-1} HCl or 1.25 mol L^{-1} NaOH. After reaction the residual concentration of Sb, Fe, and Cu in solution was determined. The individual effect of coexisting SO_4^{2-} (100–500 mg L^{-1}), PO_4^{3-} (10–100 mg L^{-1}), and CO_3^{2-} (200 mg L^{-1}) on Sb(V) removal was investigated by spiking with a certain amount of sulfate, phosphate, and carbonate separately. To assure data quality, all experiments were performed in duplicate.

2.5. Residue leach liquor collection

The Sb removal efficiency of Fe-Cu binary oxide from a real environmental sample was evaluated. Stibnite (Sb_2S_3) smelting residue was collected from Xikuangshan mine area in Hunan province of China. One hundred and fifty grams of mineral slags after milling were added to 1 L of DI water and the mixture was shaken at 100 r min^{-1} for 20 d. Then the solution were filtered through 0.45-μm membrane filters and used as leaching liquor.

2.6. Analytical methods

Total Sb, Cd, Pb, and Cu were analyzed by flame atomic absorption spectrophotometer (AA-7001, East & West Analytical Instruments, Inc., Beijing). Total Fe was determined using the 1, 10 phenanthroline spectrometric method [29].

3. Results and discussion

3.1. Particle characterization

Fig. 1 shows the SEM images of iron oxide, copper oxide, and Fe-Cu binary oxide with the Fe/Cu molar ratio of 3/1. It was found that block iron oxide and Fe-Cu binary oxide were not of uniform size, certain particles reached the nanometer grade, and some were greater than 10 μm. However, the structure of copper oxide was relatively flocculent loose.

As presented in Fig. 2(a), XRD patterns of iron oxide exhibited diffraction peaks approximately at 35°, 55°, and 62.5°, which were feature of poorly ordered ferrihydrite [30]. The characteristic peaks in copper oxide which appeared at 36.5°, 39°, 49.5°, and 62° were in good agreement with those of the standard patterns of CuO [31]. The Fe-Cu binary oxide was complex,

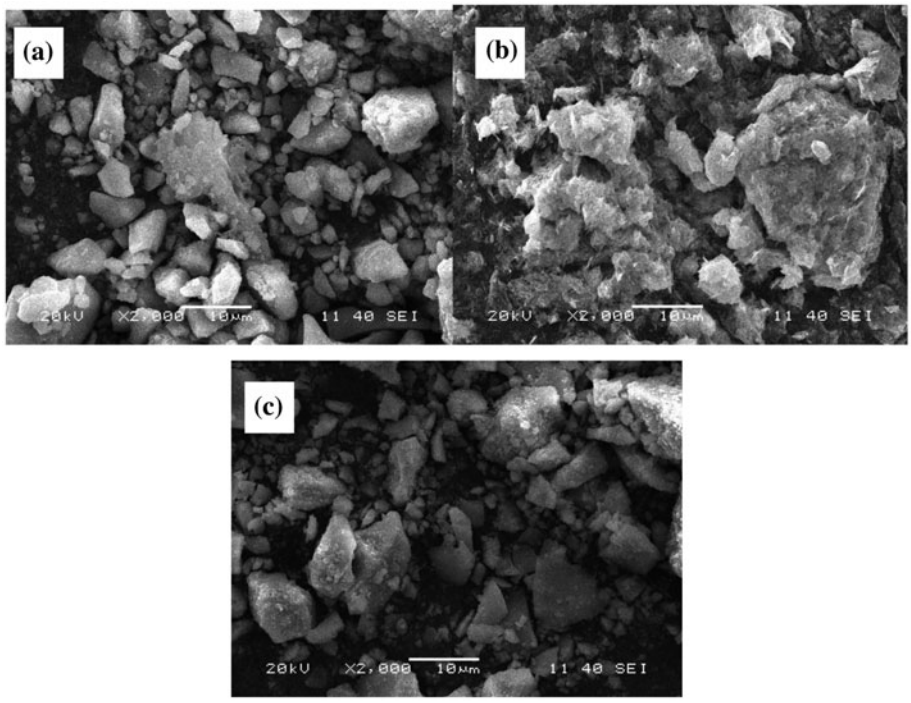

Fig. 1. SEM images of prepared (a) iron oxide, (b) copper oxide, and (c) Fe-Cu binary oxide with the Fe/Cu molar ratio of 3/1.

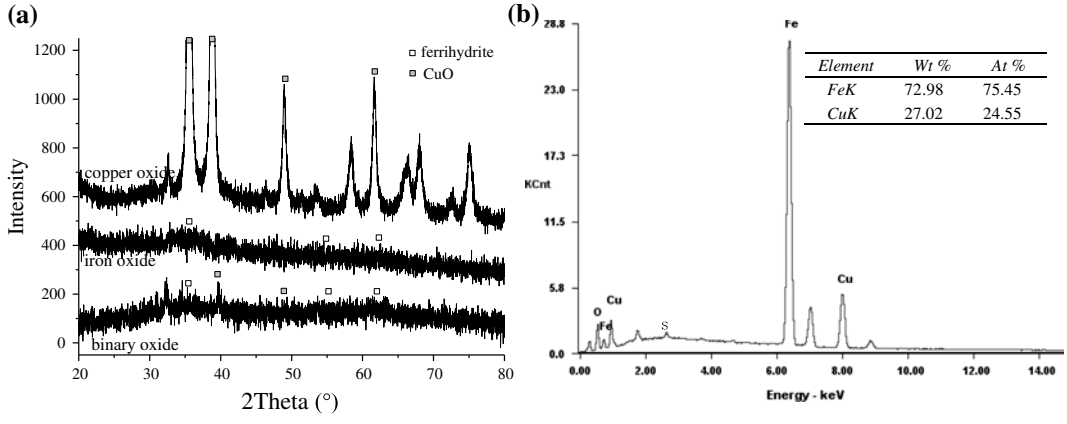

Fig. 2. (a) XRD spectra of prepared iron oxide, copper oxide, and binary oxide with Fe/Cu molar ratio of 3/1 and (b) EDX spectra of prepared Fe-Cu binary oxide with the Fe/Cu molar ratio of 3/1.

and most of the characteristic peaks coincided with that of ferrihydrite. Besides, diffraction peaks of CuO were also found. EDX analysis (Fig. 2(b)) confirmed that Fe, Cu, O, and S were the main elemental composition of Fe-Cu binary oxide. Moreover, the results revealed that the atomic ratio of element Fe/Cu for the prepared binary oxide was 3.07–1.0. And it agreed well with the theoretical value (3.0–1.0), indicating that the preparation method for the binary oxides had a good reliability.

N_2 adsorption–desorption isotherms and pore size distribution of the prepared samples are shown in Fig. 3. The BET surface area of Fe-Cu binary oxide with the Fe/Cu molar ratio of 3/1, iron oxide, and copper oxide were calculated to be 238.79, 82.39, and 28.13 $m^2 g^{-1}$, respectively. Obviously, compared to the iron oxide and copper oxide, the surface area of Fe-Cu binary oxide showed an increase.

Fig. 4 illustrates the FTIR spectra of prepared binary oxide with the Fe/Cu molar ratio of 3/1. The peak

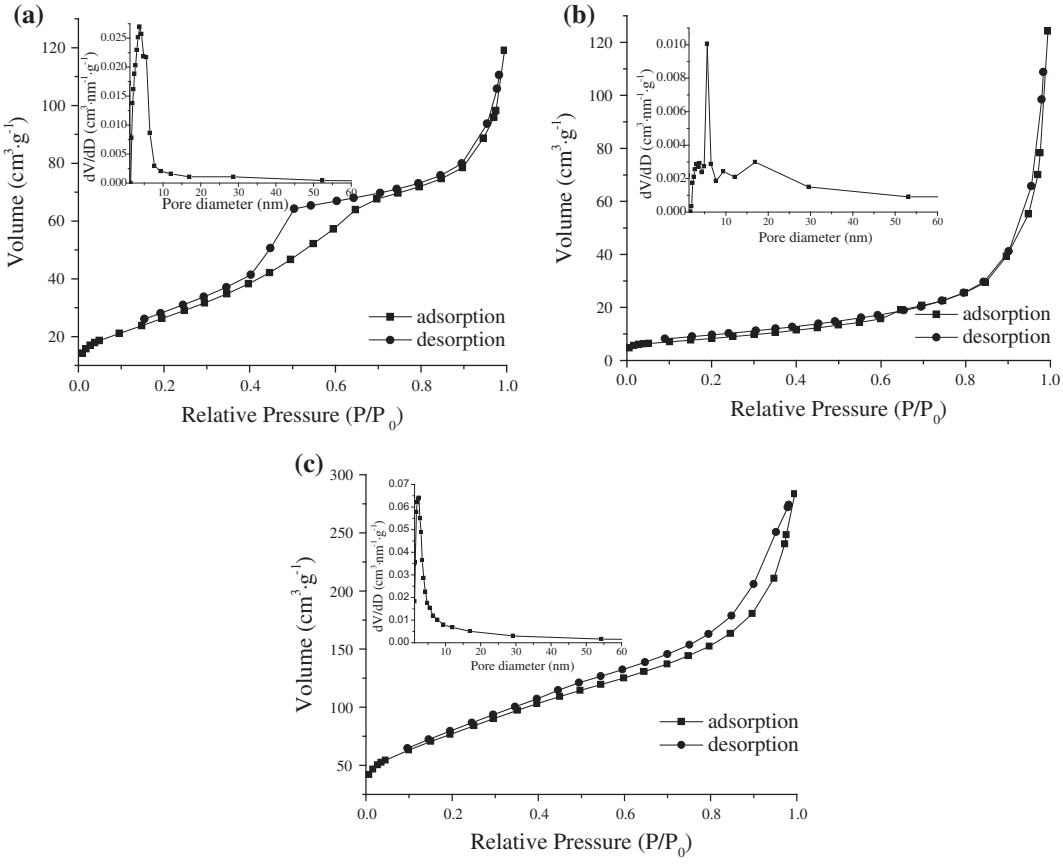

Fig. 3. N_2 adsorption–desorption isotherm and pore size distribution curve of (a) iron oxide, (b) copper oxide, and (c) Fe-Cu binary oxide with the Fe/Cu molar ratio of 3/1.

at 3,450 cm^{-1} would be assigned to the stretching vibration of –OH band [32]. The band near to 1,630 cm^{-1} was ascribed to the deformation of water molecules. The band at 1,210 and 1,070 cm^{-1} referred to –S=O stretching vibrations in sulfate [33]. The peaks between 1,070 and 980 cm^{-1} corresponded to the bending vibration of the hydroxyl group associated with Fe and Cu. And two bands at about 490–620 cm^{-1} referred to Cu–O and 2 characteristic absorption peaks [24,32].

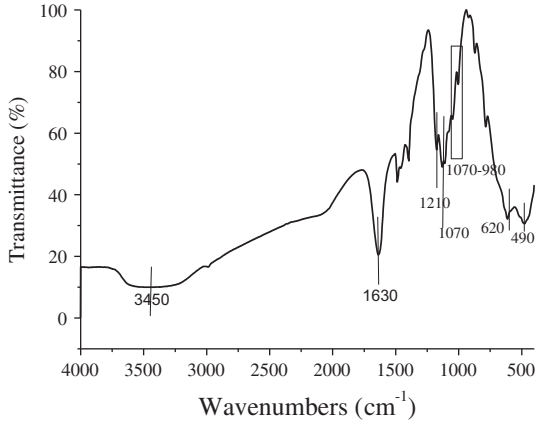

Fig. 4. FTIR spectra of the binary oxide with Fe/Cu molar ratio of 3/1.

Additionally, the analysis of zeta potential (Fig. 5) indicated that the point of zero charge of Fe-Cu binary oxide in presence of 0.01 M NaCl was about pH 7.7. It was consistent with the results reported previously for similarly prepared Fe-Cu binary oxide [27].

3.2. Fe/Cu molar ratio affecting Sb(V) removal by Fe-Cu binary oxides

A serial of Fe-Cu binary oxides with Fe/Cu molar ratios at 1/2, 1/1, 2/1, and 3/1 were synthesized. Then 0.03 g of binary oxides with different Fe/Cu molar ratio were used to remove 100 mL of 20 mg L^{-1} Sb(V) from water. Control tests in the presence of iron oxide and copper oxide were also carried out. As shown in Fig. 6, 65.6% of Sb(V) was removed by pure

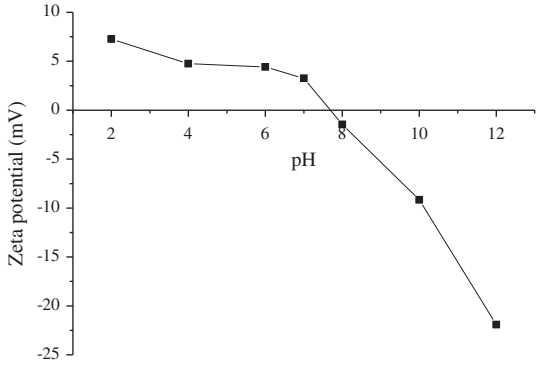

Fig. 5. Zeta potential of the binary oxide with Fe/Cu molar ratio of 3/1 over a wide pH range.

iron oxide after 24 h reaction, and only 27.7% of Sb(V) was removed by pure copper oxide. However, the Sb (V) removal rate of Fe-Cu binary oxide was higher that of both iron oxide and copper oxide at the same reaction condition. And the Sb(V) removal rate of binary oxide with Fe/Cu molar ratio of 3/1 suddenly reached to 97%. Whereas, with continue increasing copper oxide percentage, the Sb(V) removal rate of binary oxide with Fe/Cu molar ratio of 2/1, 1/1, and 1/2 decreased to 87.6, 80.6, and 79.6% correspondingly. The greater surface area of Fe-Cu binary oxide was the main reason for the high adsorption capacity of Sb(V). However, an excessive CuO content in the binary oxide was not beneficial to Sb(V) uptake, mainly because the adsorption ability of pure copper oxide was low and the iron oxide dominated in

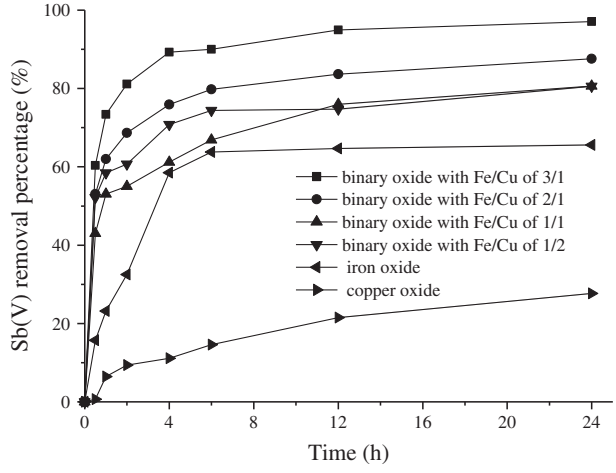

Fig. 6. Effect of Fe/Cu molar ratio on Sb(V) sorption by Fe-Cu binary oxide. Initial Sb(V) concentration was 20 mg L^{-1}, sorbent dose was 0.3 g L^{-1}, and the pH was 6.0 ± 0.1.

adsorption of Sb(V). In brief, the Fe/Cu molar ratio had a great influence on the adsorption capacity of Fe-Cu binary oxide. The optimum Fe/Cu molar ratio for binary oxide was 3/1 and it was used in the following experiments.

3.3. Kinetics of Sb(V) adsorption on Fe-Cu binary oxide

Sb(V) removal data by the binary oxide with Fe/Cu molar ratio of 3/1 at different adsorbent dose is shown in Fig. 7(a). It was found that at the Fe-Cu binary oxide dose of 0.1, 0.2, 0.3, and 0.4 g/L, about 36.17, 55.71, 82.92, and 88.85% of 40 mg/L Sb(V) were removed within 24 h, respectively. It was clear that the Sb(V) removal efficiency increased with the increase of Fe-Cu binary oxide dose. Furthermore, the removal percentage of Sb(V) increased rapid before 4 h reaction, and then slowed down as equilibrium was approached. The initial high removal rate may be attributed to the existence of large number of adsorption sites on the surface of Fe-Cu binary oxide. As the sites filled up gradually, the adsorption became slow [34].

Sb(V) removal by the Fe-Cu binary oxide was described by pseudo-second-order kinetic according to Eq. (2) [35]:

$$\frac{t}{q_t} = \frac{1}{kq_e^2} + \frac{t}{q_e} \tag{2}$$

where t (h) is the reaction time, q_e (mg g^{-1}) and q_t (mg g^{-1}) are the amount of adsorbed Sb(V) at equilibrium and at any time t, k (g mg^{-1} h^{-1}) is the equilibrium rate constant. The linear plots of t/q_t vs. t for the pseudo-second-order model at different experimental conditions are shown in Fig. 7(b). And the fitted kinetic parameters are shown in Table 1. It was found that values of the determination coefficient (R^2) were in range of 0.9942–0.9992 and the theoretical $q_{e,cal}$ values were closer to the experimental $q_{e,exp}$ values. It can be concluded that Sb(V) adsorption with Fe-Cu binary oxide did follow a pseudo-second-order kinetic, and chemical sorption played a major role in Sb(V) removal. Furthermore, the FTIR analysis which indicated the appearance of massive active hydroxyl group can support for this view.

3.4. Adsorption isotherms

Both the Langmuir and Freundlich models were used to describe the equilibrium adsorption behavior of Sb(V). The Langmuir model assumed that there

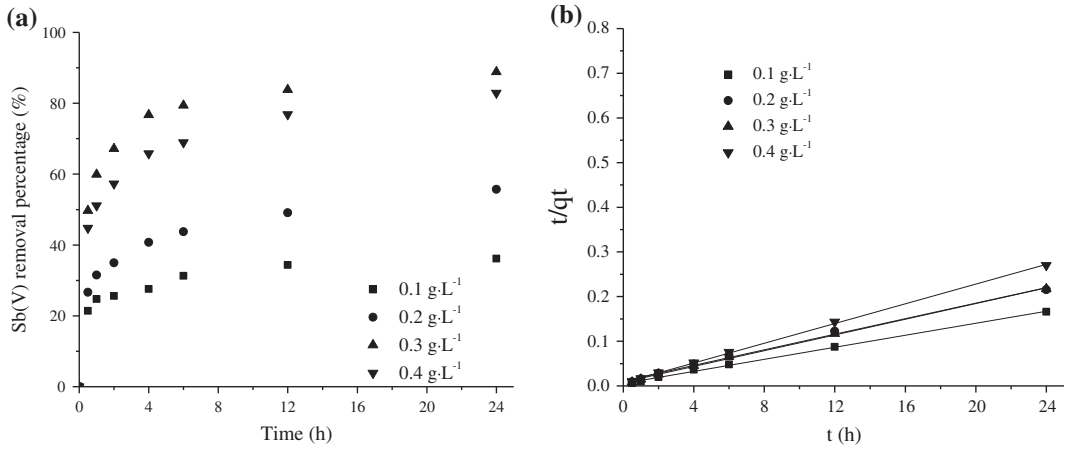

Fig. 7. (a) Trends of Sb(V) removal by the Fe-Cu binary oxide as a function of reaction time and (b) pseudo-second-order kinetic plots for Sb(V) adsorption. Initial Sb(V) concentration was 40 mg L^{-1}, the adsorbent dose was 0.1–0.4 g L^{-1}, and the solution pH was 6.0 ± 0.1.

Table 1
Kinetic constants obtained from pseudo-second-order model at different reaction condition

			Pseudo-second-order		
Dose (g L^{-1})	C_0 (mg L^{-1})	$q_{e,exp}$ (mg g^{-1})	k (g m^{-1} h^{-1})	$q_{e,cal}$ (mg g^{-1})	R^2
0.1	40	144.67	0.008	149.25	0.9978
0.2	40	111.47	0.007	114.94	0.9942
0.3	40	110.56	0.009	113.64	0.9977
0.4	40	88.85	0.017	90.91	0.9992

was no interaction between the adsorbate molecules and the adsorption was localized in a monolayer [36]. The Freundlich model assumed that different sites with several adsorption energies were involved [37]. The Langmuir and Freundlich equations are represented as Eqs. (3) and (4), respectively:

$$\frac{1}{q_e} = \frac{1}{K_L C_e q_m} + \frac{1}{q_m} \tag{3}$$

$$\ln q_e = \ln K_f + \frac{1}{n} \ln C_e \tag{4}$$

where q_e is the adsorption capacity at equilibrium (mg g^{-1}), C_e is the equilibrium concentration of Sb(V) in the aqueous solution (mg L^{-1}), q_m is the maximum sorption capacity (mg g^{-1}), K_L is the Langmuir sorption constant. K_f and n are the Freundlich constants which are indicators of adsorption capacity and adsorption intensity, respectively.

The linear equations of Langmuir and Freundlich models are tested against experimental data and presented in Fig. 8. The adsorption constants obtained are presented in Table 2. It was shown that the Freundlich model fitted the data much better than the Langmuir model in this experiment. And it is possible that the simultaneous presence of iron oxide and copper oxide in the binary oxide led to a heterogeneous surface of the Fe-Cu binary oxide. Therefore, the sorption sites on the surface of Fe-Cu binary oxide had different sorption energies. However, the Langmuir isotherm model was used satisfactorily to well describe Sb adsorption on bentonite [16], Fe-Zr bimetal oxide [22] and iron oxyhydroxides [38] elsewhere.

In addition, the adsorption capacity of Fe-Cu binary oxide at equilibrium can reach 191.9 mg g^{-1} with the initial Sb(V) concentration of 90 mg L^{-1}. And this material exhibited higher adsorption capacity than many other adsorbents that had been reported before. Such as the maximal removal capability of Sb(V) by

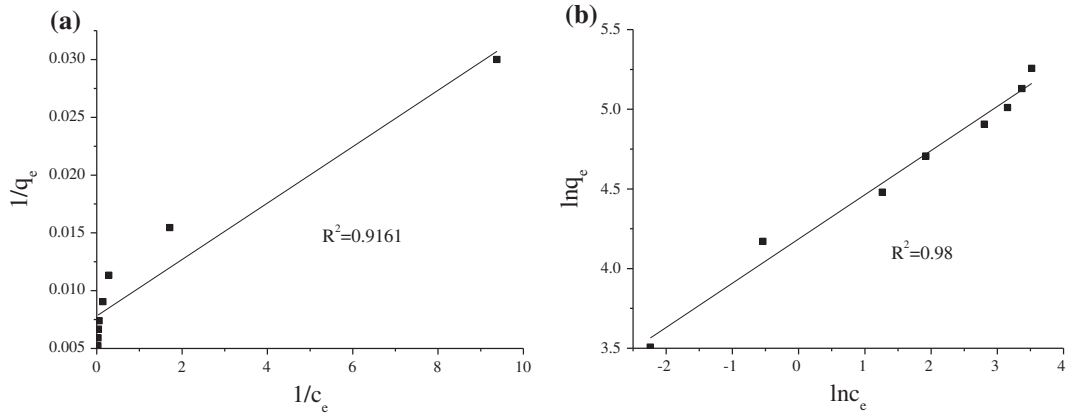

Fig. 8. (a) Langmuir and (b) Freundlich isotherm plots for Sb(V) adsorption. Initial Sb(V) concentration was 10–90 mg L^{-1}, adsorbent dose was 0.3 g L^{-1}, and solution pH was 6.0 ± 0.1.

Table 2
Langmuir and Freundlich isotherm parameters of Sb(V) adsorption to Fe-Cu binary oxide

Langmuir			Freundlich		
q_{max} (mg g^{-1})	K_L (L mg^{-1})	R^2	$1/n$	K_F (g mg^{-1} L^{-1})	R^2
128.04	3.2	0.9161	0.277	65.75	0.98

nanoscale zero-valent iron stabilized by polyvinyl alcohol was 1.65 mg g^{-1} at pH 7.0 [19], the maximum adsorption capacity of Sb(V) by Fe-Mn binary oxide was 127.89 mg g^{-1} at pH 5.0 [21], the maximal removal capability of Sb(V) by Fe-Zr bimetal oxide was 51 mg g^{-1} at pH 7.0 [22], and the maximal removal capability of Sb(V) by hydrous ferric oxide was 113.95 mg g^{-1} at pH 4.0 [38].

3.5. Effect of solution pH on Sb(V) adsorption and metal leaching of Fe-Cu binary oxide

Sb(V) removal by Fe-Cu binary oxide at four pHs (4.0 ± 0.1, 6.0 ± 0.1, 8.0 ± 0.1, and 10.0 ± 0.1) was conducted. Fig. 9(a) demonstrats that when the initial pH increased from 4.0 to 10.0, the Sb(V) removal rate decreased from 92.82 to 67.88%. After reaction solution pH raised a bit which had little effect on Sb(V) removal. It was known that, negatively charged $Sb(OH)_6^-$ and SbO_3^- were the dominated species of Sb (V) when the pH was more than 3.0 [1]. Whereas, as the pH increased, the negatively charged sites on the binary oxide surface increased (Fig. 4), which increased the repulsive force between the negatively charged Sb(V) species and the binary oxide surface. Therefore, the adsorption capacity of binary oxide decreased with the increasing of solution pH.

Fig. 9(b) demonstrates the concentrations of dissolved Fe and Cu in water after reaction under different pHs. It was shown that the leaching of Fe and Cu was serious under acid condition. However, when the pH was more than 4.0, the Fe concentrations were all below the limit (0.3 mg L^{-1}) of drinking water standard of China [39]. When the pH was more than 6.0, the Cu concentrations were all below the limit of drinking water of 1 mg L^{-1}. Obviously, the prepared sorbent release was very small in pH range of 6.0–9.0, and it can be safely used in the majority of waters.

3.6. Effect of coexisting anions on Sb(V) adsorption

The individual effect of coexisting SO_4^{2-}, PO_4^{3-}, and CO_3^{2-} on Sb(V) removal is shown in Fig. 10. It was found that CO_3^{2-} had little effect on Sb(V) sorption on Fe-Cu binary oxide. Compared with DI water, the Sb (V) removal rate decreased by 9.13, 14.35, and 18.62% in the presence of 100, 300, and 500 mg L^{-1} SO_4^{2-}, respectively. And the Sb(V) removal rate decreased by 12.46, 24.54, and 33.28% in the presence of 10, 50, and 100 mg L^{-1} PO_4^{3-}, respectively. It was shown that the sorption ability of Fe-Cu binary oxide decreased in the presence of high concentration of sulfate which might occur in Sb_2S_3 mine drainage. However, the present PO_4^{3-} hindered Sb(V) sorption significantly, even at low concentration levels. It was because there was strong competition for the binding sites of the sorbent between PO_4^{3-} and $Sb(OH)_6^-$ [20].

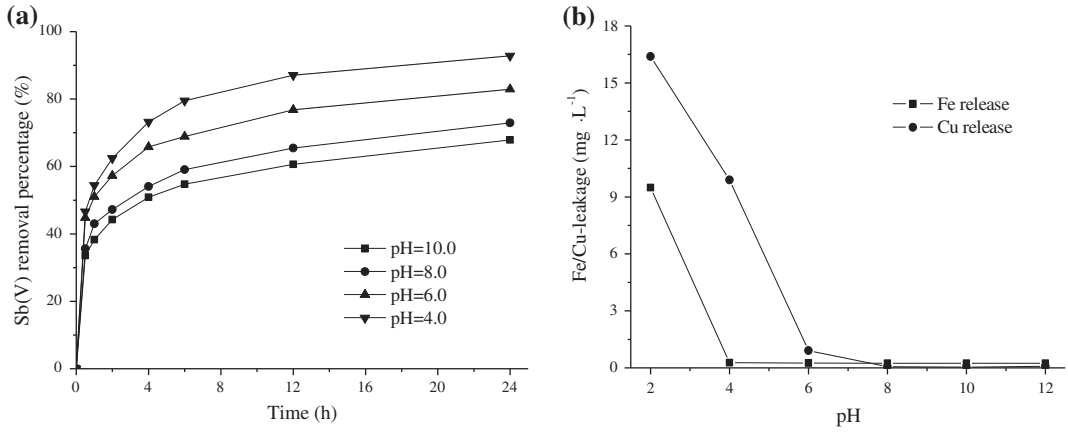

Fig. 9. (a) Effect of solution pH on the sorption ability of Fe-Cu binary oxide and (b) release of Fe and Cu to water after reaction. Initial Sb(V) concentration was 40 mg L^{-1}, binary oxide dose was 0.3 g L^{-1}, and solution pH was 6.0 ± 0.1.

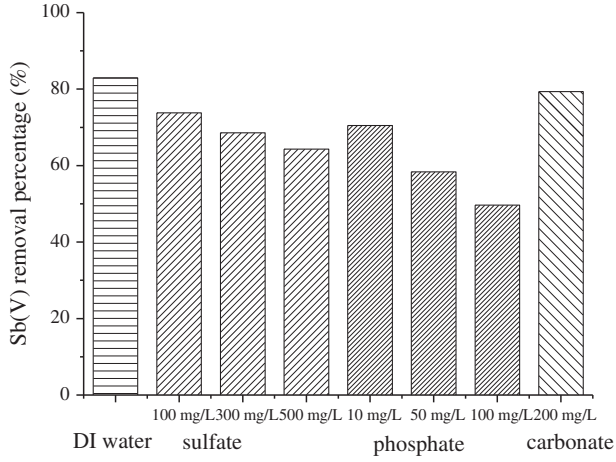

Fig. 10. Effect of coexisting anions SO_4^{2-}, CO_3^{2-}, and PO_4^{3-} on Sb(V) adsorption. Initial Sb(V) concentration was 40 mg L^{-1}, binary oxide dose was 0.3 g L^{-1}, and solution pH was 6.0 ± 0.1.

3.7. Mechanism of Sb(V) removal by Fe-Cu binary oxide

After reaction the Fe-Cu binary oxide was recovered and characterized by the SEM. As shown in Fig. 11(a), the morphology of Fe-Cu binary oxide did change significantly after Sb(V) adsorption compared with the fresh prepared Fe-Cu binary oxide. And some crystalline block substances occurred which might be helpful for gaining a better removal capacity of Sb(V). For further analysis of chemical composition, the product was characterized with XRD (Fig. 11(b)). It can be seen that the peaks of ferrihydrite and CuO became weak after reaction. However, new peaks with high intensity at 32.5˚, 46.5˚, and 57˚ were observed, which were the characteristic peaks of $Cu_{12}Sb_4S_{13}$ based tetrahedrite [40,41]. By collecting information about the adsorbent's structure and removal ability as mentioned earlier, the removal mechanism of Sb(V) by Fe-Cu binary oxide could be concluded as follows: (1) during the first 4 h Sb(V) was adsorbed immediately to Fe-Cu binary oxide and iron oxide acted as the main adsorption site; (2) as the reaction continued, the dissolution of Fe-Cu binary oxides happened and some Fe^{3+} and Cu^{2+} ions were released to the water; (3) then the Fe^{3+} and Cu^{2+} were readsorbed to the binary oxide, and the iron-substituted tetrahedrite ($Cu_{12-x}Fe_xSb_4S_{13}$) was formed.

3.8. Treatment of antimony residue leach liquor

It was very important to use the Fe-Cu binary oxide to remove Sb from a real environmental sample. Therefore, the ore leaching liquor was collected as mentioned above. The pH of leach liquor was 7.22, and total Sb, Cd, and Pb concentration was 37.03, 0.29, and 0.34 mg L^{-1}, respectively. Coexisting SO_4^{2-} concentration was 958.45 mg L^{-1}. Then 0.03 g Fe-Cu binary oxides were added to the 100 mL wastewater. After 48 h of reaction, the solution pH increased to 7.45–37.74% of Sb was removed. Correspondingly, the Sb removal capacity of Fe-Cu binary oxide from the residue leach liquor was about 46.58 mg g^{-1}. However, it was seriously decreased compared with the Sb removal from DI water. There were two reasons for this. First, the coexisting SO_4^{2-} in antimony mine drainage was as high as hundreds of mg L^{-1} [42,43] and significantly reduced the Sb removal rate. Second, multiple heavy metals were commonly associated in stibnite [42,44], and therefore a certain amount of Cd and Pb presented in the leaching liquor could compete with Sb(V) for the same binding sites available on Fe-Cu binary oxides' surfaces [45].

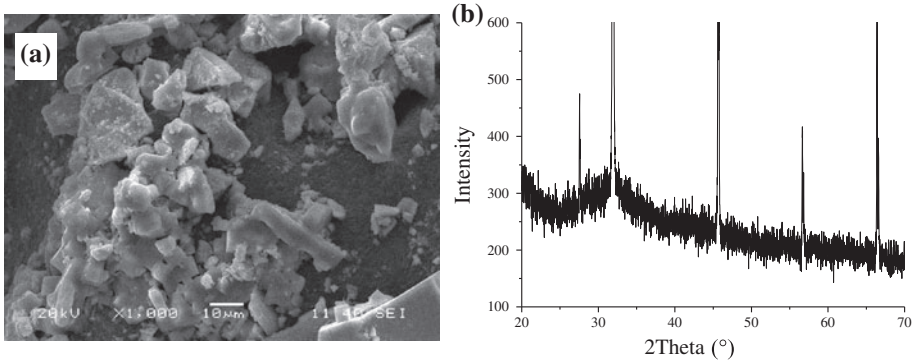

Fig. 11. (a) SEM image and (b) XRD pattern of Fe-Cu binary oxide after Sb(V) adsorption reaction. Initial Sb(V) concentration was 40 mg L^{-1}, binary oxide dose was 0.3 g L^{-1}, and the pH was 6.0 ± 0.1.

4. Conclusions

In this study, Fe-Cu binary oxides with different Fe/Cu mole ratio were successfully prepared through a simple co-precipitation method. And these adsorbents were characterized using SEM, EDX, and XRD, N_2 adsorption–desorption as well as FTIR method. The results indicated that the synthetic Fe-Cu binary oxide was amorphous and consisted of ferrihydrite and CuO. The adsorption performances of binary oxides with different Fe/Cu mole ratio were investigated carefully. It was found that the binary oxide with Fe/Cu molar ratio of 3/1 had the highest removal rate of Sb(V). Kinetic results revealed that Sb (V) sorption onto Fe-Cu binary oxide followed a pseudo-second-order kinetic model. Freundlich model fitted the adsorption equilibrium data better than the Langmuir model. The maximal adsorption capacity of Fe-Cu binary oxides toward Sb(V) was 191.9 mg g^{-1} at pH 6.0, which was higher than many other reported adsorbents. Moreover, the Sb(V) removal rate decreased with increased pH value. Coexisting anions SO_4^{2-} and PO_4^{3-} had effect on the Sb(V) adsorption. Although the Sb removal capacity of Fe-Cu binary oxide from the residue leach liquor was lower than DI water, it was certainly a promising adsorbent for antimony removal from contaminated water.

Acknowledgments

This work was supported by the National Nature Science Foundation of China (No. 51504094 and 51308209), the Research Foundation of Education Department of Hunan Province, China (No. 13C310), the Science Foundation of Hunan University of Science and Technology for the introduction of specialized personnel with doctorates (No. E51362).

References

[1] M. Filella, N. Belzile, Y.W. Chen, Antimony in the environment: A review focused on natural waters. II. Relevant solution chemistry, Earth Sci. Rev. 59 (2002) 265–285.
[2] United States Environmental Protection Agency, Water Related Fate of the 129 Priority Pollutants. vol. 1, USEPA, EP-440r4-79-029A, Washington, DC, 1979.
[3] K. Telford, W. Maher, F. Krikowa, S. Foster, M.J. Ellwood, P.M. Ashley, P.V. Lockwood, S.C. Wilson, Bioaccumulation of antimony and arsenic in a highly contaminated stream adjacent to the Hillgrove Mine, NSW, Australia, Environ. Chem. 6 (2009) 133–143.
[4] M. Filella, P.A. Williams, N. Belzile, Antimony in the environment: Knowns and unknowns, Environ. Chem. 6 (2009) 95–105.
[5] M.C. He, X.Q. Wang, F.C. Wu, Z.Y. Fu, Antimony pollution in China, Sci. Total Environ. 421–422 (2012) 41–50.
[6] I. Ondrejková, Z. Ženišová, R. Fľaková, D. Krčmář, O. Sracek, The distribution of antimony and arsenic in waters of the Dúbrava abandoned mine site, Mine Water Environ. 32 (2013) 207–221.
[7] H.G. Sigel, A. Sigel, H. Sigel, Handbook on Metals in Clinical and Analytical Chemistry, Marcel Dekker Inc., New York, NY, 1994, pp. 227–236.
[8] G. Ceriotti, D. Amarasiriwardena, A study of antimony complexed to soil-derived humic acids and inorganic antimony species along a Massachusetts highway, Microchem. J. 91 (2009) 85–93.
[9] S. Ackermann, R. Gieré, M. Newville, J. Majzlan, Antimony sinks in the weathering crust of bullets from Swiss shooting ranges, Sci. Total Environ. 407 (2009) 1669–1682.
[10] R.P. Liu, W. Xu, Z. He, H.C. Lan, H.J. Liu, J.H. Qu, T. Prasai, Adsorption of antimony(V) onto Mn(II)-enriched surfaces of manganese-oxide and Fe-Mn binary oxide, Chemosphere 138 (2015) 616–624.
[11] M.S. Oncel, A. Muhcu, E. Demirbas, M. Kobya, A comparative study of chemical precipitation and electrocoagulation for treatment of coal acid drainage wastewater, J. Environ. Chem. Eng. 1 (2013) 989–995.

[12] X.J. Guo, Z.J. Wu, M.C. He, Removal of antimony(V) and antimony(III) from drinking water by coagulation-flocculation-sedimentation (CFS), Water Res. 43 (2009) 4327–4335.
[13] M.E.H. Bergmann, A.S. Koparal, Electrochemical antimony removal from accumulator acid: Results from removal trials in laboratory cells, J. Hazard. Mater. 196 (2011) 59–65.
[14] B.K. Biswas, J.I. Inoue, H. Kawakita, K. Ohto, K. Inoue, Effective removal and recovery of antimony using metal-loaded saponified orange waste, J. Hazard. Mater. 172 (2009) 721–728.
[15] G. Ungureanu, S. Santos, R. Boaventura, C. Botelho, Arsenic and antimony in water and wastewater: Overview of removal techniques with special reference to latest advances in adsorption, J. Environ. Manage. 151 (2015) 326–342.
[16] J.H. Xi, M.C. He, C.Y. Lin, Adsorption of antimony (III) and antimony(V) on bentonite: Kinetics, thermodynamics and anion competition, Microchem. J. 97 (2011) 85–91.
[17] M.A. Salam, R.M. Mohamed, Removal of antimony (III) by multi-walled carbon nanotubes from model solution and environmental samples, Chem. Eng. Res. Des. 91 (2013) 1352–1360.
[18] T.C. Yu, X.H. Wang, C. Li, Removal of antimony by FeCl3-modified granular-activated carbon in aqueous solution, J. Environ. Eng. 140 (2014) A4014001–1.
[19] X.Q. Zhao, X.M. Dou, D. Mohan, C.U. Pittman, Y.S. OK, X. Jin, Antimonate and antimonite adsorption by a polyvinyl alcohol-stabilized granular adsorbent containing nanoscale zero-valent iron, Chem. Eng. J. 6 (2014) 4268–4274.
[20] F. Kolbe, H. Weiss, P. Morgenstern, R. Wennrich, W. Lorenz, K. Schurk, H. Stanjek, B. Daus, Sorption of aqueous antimony and arsenic species onto akaganeite, J. Colloid Interface Sci. 357 (2011) 460–465.
[21] W. Xu, R.P. Liu, J.H. Qiu, R.M. Peng, The adsorption behaviors of Fe-Mn binary oxide towards Sb(V), Acta Scientiae Circumstantiae 32 (2012) 270–275.
[22] X.H. Li, X.M. Dou, J.Q. Li, Antimony(V) removal from water by iron-zirconium bimetal oxide: Performance and mechanism, J. Environ. Sci. 24 (2012) 1197–1203.
[23] H.T. Lu, Z.L. Zhu, H. Zhang, J.Y. Zhu, Y.L. Qiu, Simultaneous removal of arsenate and antimonate in simulated and practical water samples by adsorption onto Zn/Fe layered double hydroxide, Chem. Eng. J. 276 (2015) 365–375.
[24] R. Sankar, P. Manikandan, V. Malarvizhi, T. Fathima, K.S. Shivashangari, V. Ravikumar, Green synthesis of colloidal copper oxide nanoparticles using Carica papaya and its application in photocatalytic dye degradation, Spectrochim. Acta Part A 121 (2014) 746–750.
[25] E. Alonso, C. Pérez-Rábago, J. Licurgo, E. Fuentealba, C.A. Estrada, First experimental studies of solar redox reactions of copper oxides for thermochemical energy storage, Sol. Energy 115 (2015) 297–305.
[26] C.A. Martinson, K.J. Reddy, Adsorption of arsenic(III) and arsenic(V) by cupric oxide nanoparticles, J. Colloid Interface Sci. 336 (2009) 406–411.
[27] G.S. Zhang, Z.M. Ren, X.W. Zhang, J. Chen, Nanostructured iron(III)-copper(II) binary oxide: A novel adsorbent for enhanced arsenic removal from aqueous solutions, Water Res. 47 (2013) 4022–4031.
[28] G.L. Li, S. Gao, G.S. Zhang, X.W. Zhang, Enhanced adsorption of phosphate from aqueous solution by nanostructured iron(III)–copper(II) binary oxides, Chem. Eng. J. 235 (2014) 124–131.
[29] APHA-AWWA-WEF, Standard Methods for Examination of Water and Wastewater, twentyth ed., American Public Health Association, Washington, DC, 1998.
[30] U. Schwertmann, R.M. Cornell, Iron Oxides in the Laboratary, second ed., WileyeVCH, Weinheim, 2000.
[31] M.H. Habibi, B. Karimi, Application of impregnation combustion method for fabrication of nanostructure CuO/ZnO composite oxide: XRD, FESEM, DRS and FTIR study, J. Ind. Eng. Chem. 20 (2014) 1566–1570.
[32] W. Xu, H.J. Wang, R.P. Liu, X. Zhao, J.H. Qu, The mechanism of antimony(III) removal and its reactions on the surfaces of Fe-Mn Binary Oxide, J. Colloid Interface Sci. 363 (2011) 320–326.
[33] V. Bhardwaj, P. Sharma, M.S. Chauhan, S. Chauhan, Thermodynamic, FTIR, ^{1}H-NMR, and acoustic studies of butylated hydroxyanisole and sodium dodecyl sulfate in ethanol, water rich and ethanol rich solutions, J. Mol. Liq. 180 (2013) 192–199.
[34] B. Geng, Z.H. Jin, T.L. Li, X.H. Qi, Kinetics of hexavalent chromium removal from water by chitosan-Fe^{0} nanoparticles, Chemosphere 75 (2009) 825–830.
[35] Y.S. Ho, G. McKay, Pseudo-second-order model for sorption processes, Process Biochem. 34 (1999) 451–465.
[36] I. Langmuir, The adsorption of gases on plane surfaces of glass, mica and platinum, J. Am. Chem. Soc. 40 (1918) 1361–1403.
[37] H.M.F. Freundlich, Uber die adsorption in Lösungen, J. Phys. Chem. 57 (1906) 385–470.
[38] X.J. Guo, Z.J. Wu, M.C. He, X.G. Meng, X. Jin, N. Qiu, J. Zhang, Adsorption of antimony onto iron oxyhydroxides: Adsorption behavior and surface structure, J. Hazard. Mater. 276 (2014) 339–345.
[39] Standardization Administration of the People's Republic of China, Standards for Drinking Water Quality (GB5749-2006), Beijing, 2006.
[40] P. Maiello, G. Zoppi, R.W. Miles, N. Pearsall, I. Forbes, Chalcogenisation of Cu-Sb metallic precursors into $Cu_3Sb(Se_xS_{1-x})_3$, Sol. Energy Mater. Sol. Cells 113 (2013) 186–194.
[41] T. Barbier, P. Lemoine, S. Gascoin, O.I. Lebedev, A. Kaltzoglou, P. Vaqueiro, A.V. Powell, R.I. Smith, E. Guilmeau, Structural stability of the synthetic thermoelectric ternary and nickel-substituted tetrahedrite phases, J. Alloys Compd. 634 (2015) 253–262.
[42] J. Zhu, F.C. Wu, Q.J. Deng, S.X. Shao, C.L. Mo, X.L. Pan, W. Li, R.Y. Zhang, Environmental characteristics of water near the Xikuangshan antimony mine, Hunan Province, Acta Scientiae Circumstantiae 29 (2009) 655–661.
[43] X.Q. Wang, M.C. He, J.H. Xi, X.F. Lu, Antimony distribution and mobility in rivers around the world's largest antimony mine of Xikuangshan, Hunan Province, China, Microchem. J. 97 (2011) 4–11.
[44] C.L. Mo, F.C. Wu, Z.Y. Fu, J. Zhi, L. Ran, Antimony, arsenic and mercury pollution in agricultural soil of antimony mine area in Xikuangshan, Hunan, J. Miner. 3 (2013) 344–349.
[45] S.X. Dong, X.M. Dou, D. Mohan, C.U. Pittman, J.M. Luo, Synthesis of graphene oxide/schwertmannite nanocomposites and their application in Sb(V) adsorption from water, Chem. Eng. J. 270 (2015) 205–214.